Photoionization microscopy of the hydrogen atom in parallel electric and magnetic fields

L. Wang,[1,2] H. F. Yang,[1,2] X. J. Liu,[1] H. P. Liu,[1,*] M. S. Zhan,[1] and J. B. Delos[3]

[1]*State Key Laboratory of Magnetic Resonance and Atomic and Molecular Physics, Wuhan Institute of Physics and Mathematics, Chinese Academy of Sciences, Wuhan 430071, People's Republic of China*

[2]*Graduate School of the Chinese Academy of Sciences, Beijing 100049, People's Republic of China*

[3]*College of William and Mary, Williamsburg, Virginia 23187-8795, USA*

(Received 19 June 2010; published 30 August 2010)

In photoionization microscopy experiments, an atom in an electric field is ionized by a laser with sharply defined frequency, the electron is drawn toward a position-sensitive detector, and the current is measured as a function of position. Multiple classical paths lead from the atom to any point in the classically allowed region on the detector, and waves traveling along these paths produce an interference pattern. If a magnetic field is added parallel to the electric field, trajectories become chaotic. There is an infinite set of different families of trajectories, leading to an extremely complicated interference patterns on the detector. We present calculations predicting the kind of structure that will be seen in experiments.

DOI: 10.1103/PhysRevA.82.022514 PACS number(s): 32.80.Fb, 03.65.Sq, 07.81.+a

I. INTRODUCTION

The two-dimensional flux of electrons escaping from a photodetachment [1,2] or photoionization process [3–6] in the presence of an electric field has been measured using a position-sensitive detector located at a macroscopic distance. The flux measurements display circular rings of interference on the detector. The interference pattern results from electron waves traveling along different classical paths from the ion or atom to the detector [7–10]. In the case of photodetachment, the escaping electron is subject only to the constant applied electric field. Only two paths go from the ion to any point on the detector, and the resulting electron distribution on the detector is a regular two-term interference pattern.

Recently, much attention has been paid to photodetachment microscopy in the presence of parallel electric and magnetic fields [11–13]. Photodetachment in parallel fields is simple enough to permit analytic quantum and semiclassical solution. The motion of the electron undergoes uniformly accelerated motion along the symmetry axis while orbiting on a circular track in the perpendicular plane. There is a finite number of interfering classical trajectories, depending on the energy and applied field strengths, and on the location of the detector.

Photoionization microscopy is much more complex [5,14,15]. First, the escaping electron is affected both by the electric field and the long-range Coulomb field of the residual ion. The resulting trajectories are more complex than in the case of photodetachment, and an infinite number of classical trajectories arrive at any point in the classically allowed region on the detector. Second, for photoionization of hydrogen atoms, the situation has a further complication. At each energy and electric field, there is a critical angle such that trajectories leaving the ion with an initial angle below (downhill from) that critical angle arrive rather quickly at the detector, but those leaving with an initial angle above (uphill from) that critical angle stay forever in the vicinity of the ion. Those uphill trajectories, bound forever in classical mechanics, correspond to quasibound resonances in quantum mechanics. Electrons in such resonance states eventually tunnel through an effective potential-energy barrier, escape toward the detector, and may produce a strong and distinctive pattern. The number of oscillations in this pattern matches a quantum number of the quasibound state. Many of these resonances are long lived, and might not give any signal in photoionization microscopy experiments, but some of them have short enough lifetimes that they may give a large signal. Therefore the signal at the detector is a combination of "background" interferences involving an infinite number of "downhill" trajectories together with distinctive patterns arising from resonances. The background contribution varies smoothly with energy, but the resonance contributions change dramatically near the energy of each resonance. This behavior was predicted in a series of papers by Kondratovich and Ostrovsky [10], and detailed calculations were carried out by Zhao and Delos [16,17].

Photoionization microscopy observed for nonhydrogenic atoms such as xenon is quite different from the theoretical predictions for hydrogen [5]. It was found that the interference pattern has smooth evolution with energy, and there is no evidence of resonances. Presumably, for such large atoms, electron scattering from the residual ion core reduces the lifetimes of the resonances so that they become indistinguishable from the background. Bordas *et al.* extend the semiclassical model described by Kondratovich and Ostrovsky for hydrogen atom in an electric field, and present numerical simulations in reasonable agreement with the experimental results [14,16,17].

Inspired by these works, we present here a study of a more complex case, photoionization microscopy for atoms in parallel electric and magnetic fields. At low energies and weak electric and magnetic fields, where the Coulomb force dominates, properties of the bound states have been found using various forms of perturbation theory or by accurate numerical computations [18–21]. The spectrum is described in terms of three classes of eigenstates, which correspond to the semiclassical quantization of three classes of regular bound trajectories. At higher energies, in the chaotic region, the absorption spectrum was studied using closed orbit theory by Mao *et al.* [22] and by Courtney [23].

The present paper complements this work by studying orbits that escape from the atom rather than orbits that return

*liuhongping@wipm.ac.cn

to it. As the electron escapes from the residual ion, all three forces, electric, magnetic, and Coulomb, have comparable magnitudes, trajectories are chaotic, and escape is described by the theory of chaotic transport [24–27]. For energies between the saddle energy and the zero-field ionization energy, it was found that trajectories leaving the ion in a downhill direction escape quickly, while those going out in an uphill direction stay close to the ion for a long time, or possibly forever. However, instead of a sharp boundary between these two types of behavior, there is a fractal boundary. Previous work explored this fractal by examining the time spectrum of escaping electrons. In this paper we explore aspects of that same fractal by examining the spatial pattern of interfering electrons on a detector. Atomic units are used unless other units are specified.

II. THEORY

The Hamiltonian of a hydrogenic electron in parallel electric and magnetic fields can be written in cylindrical coordinates (ρ,z) and in scaled units as

$$H(\rho,z,p_\rho,p_z)=\tfrac{1}{2}\left(p_\rho^2+p_z^2\right)+V(\rho,z)\equiv E, \tag{1}$$

where the z component of angular momentum is taken to be zero. The potential-energy term in the Hamiltonian can be expressed as

$$V(\rho,z)=-\frac{1}{\sqrt{\rho^2+z^2}}+z+\frac{1}{8}B^2\rho^2, \tag{2}$$

where $E=\widehat{E}\widehat{F}^{-1/2}$ and $B=\widehat{B}\widehat{F}^{-3/4}$ are the scaled energy and the scaled magnetic field strength, respectively, while $\widehat{E}$, $\widehat{F}$, and $\widehat{B}$ are the physical energy, the physical electric-field strength, and the physical magnetic-field strength (in atomic units), respectively.

Following standard practice [12,28], we define parabolic coordinates (u,v) and their conjugate momenta (p_u,p_v) by

$$u=\sqrt{r+z},\quad v=\sqrt{r-z}, \tag{3}$$

$$p_u=vp_\rho+up_z,\quad p_v=up_\rho-vp_z, \tag{4}$$

where $r=\sqrt{\rho^2+z^2}=(u^2+v^2)/2$. The inverse transformations for Eqs. (3) and (4) are

$$\rho=uv,\quad z=\frac{1}{2}(u^2+v^2), \tag{5}$$

$$p_\rho=\frac{vp_u+up_v}{u^2+v^2},\quad p_z=\frac{up_u-vp_v}{u^2+v^2}. \tag{6}$$

We introduce an effective Hamiltonian $h=2r(H-E)$, which equals

$$h(u,v,p_u,p_v)=\tfrac{1}{2}\left(p_u^2+p_v^2\right)+V_{uv}(u,v)-2, \tag{7}$$

where

$$V_{uv}(u,v)=-E(u^2+v^2)+\tfrac{1}{8}B^2(u^4v^2+u^2v^4)+\tfrac{1}{2}(u^4-v^4). \tag{8}$$

For the Hamiltonian in Eq. (7), we can perform semiclassical trajectory calculations. Our treatment is strictly limited to the semiclassical approximation and the contribution of the tunneling integral is neglected [15,16]. In the calculation, however, the Maslov index is introduced to correct the phase due to the failure of the semiclassical approximation when the momenta vanish.

In photoionization, suppose the electron in the excited state is ejected with an angle $\theta=\tan^{-1}(\rho/z)=2\tan^{-1}(v/u)$, which is defined as the angle between the initial velocity of the photoelectron and the external field, and arrives at the imaging detector located at $z=z_0$. For any point on the detector, denoted by $M(R,z_0)$, where R is the polar radius of the point on the detector surface, there exist an infinite number of photoelectron trajectories passing through it in the classically accessible region. In the semiclassical approximation, except at the caustic surfaces, the magnitude and phase of the semiclassical wave function for trajectory i, denoted by $\psi_i(R)$, depend on its classical density ρ_i and classical action functional $S_i(R,E)$:

$$\psi_i(R)=\sqrt{\rho_i(R)}\exp[i\chi_i(R)]. \tag{9}$$

Here, the phase $\chi_i(R)$ is given by

$$\chi_i(R)=S_i(R,E)\omega-\frac{\pi}{2}\mu_i(i), \tag{10}$$

$$S_i(R,E)=\int_0^M p_i\,dq_i, \tag{11}$$

where $\omega=F^{-1/4}$ and the Maslov index $\mu_i(R)$ keeps track of the singularity "history" of the trajectory where the density ρ_i diverges.

The procedure of the calculation can be summarized as follows. For given scaled energy E, magnetic field B, and detector position z_0, we model the electronic wave function, immediately after the excitation, by an ensemble of classical trajectories that begin at the nucleus and propagate radially outward in all directions with an isotropic initial electron angular distribution [3,14]. For a given R at the detector, the motion of the electron is integrated numerically in regularized coordinates with θ in small steps from 0 and π, and at each step of θ, we monitor the positions of trajectories landing at the detector $R(z_0)$. If, as θ changes, $R(z_0)$ increases or decreases past the chosen R, the integration is interrupted, and then we optimize the starting angle using a Newton procedure so that the trajectory lands on R at the detector as close as possible. Simultaneously, the ejected angle $\theta_i(R)$ is recorded and the phase $\chi_i(R)$ is calculated according to Eq. (10). We stop the integration and pass over to the next starting direction if the evolution cannot reach the detector within a set maximum period of time.

After weighting the contribution of the initial direction θ according to the density $\sin\theta$, the resulting wave function $\psi(R)$ at point $M(R,z_0)$ is subsequently obtained by summing the amplitudes over all possible trajectories, leading from the electron source to this point according to

$$\psi_{sc}(R)=\sum_i\psi_i(R)=\sum_i\left(\frac{d\theta_i(R)}{dR}\sin\theta_i(R)\right)^{1/2}\exp[i\chi_i(R)], \tag{12}$$

where θ_i represents any ejection angle leading to the detection of the electron at radius R on the detector. The calculated radial probability distribution $\rho_{sc}(R)$ is then obtained

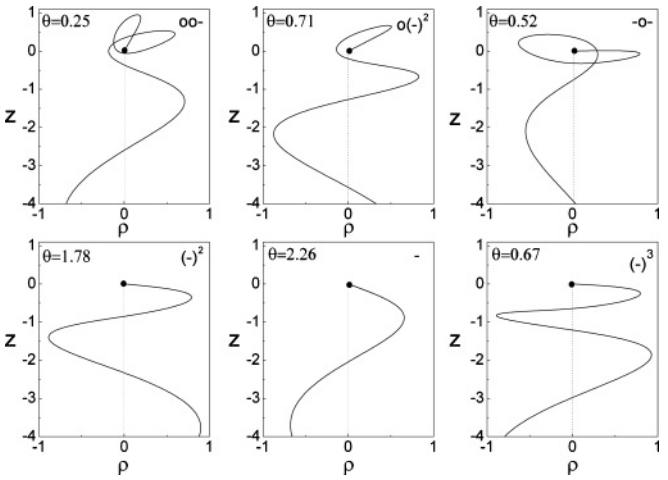

FIG. 1. Typical trajectories (ρ,z) for hydrogen in parallel electric and magnetic fields at $B = 4$, $E = 0$. The solid dots stand for the origin of the coordinates (ρ,z). The electric and magnetic fields are along the vertical z axis. The ejected angles and labels are shown in each panel.

according to

$$\rho_{sc}(R) = |\psi_{sc}(M(R,z_0))|^2 = \sum_i \rho_i + 2\sum_{i<j}\sqrt{\rho_i\rho_j}\cos(\chi_i - \chi_j). \quad (13)$$

The first term is the classical probability distribution, and the second represents interference among classical paths arriving at each point on the detector [12,28].

Following Mitchell and Delos [29], we label the qualitative behavior of ionization trajectories using a finite string of the symbols $\{-,o\}$. Each time a trajectory intersects the negative z axis, we record it as symbol o if the trajectory has encircled the nucleus since its last intersection. If it has not encircled the nucleus, we record it as symbol $-$. We record the symbols from left to right, beginning with the first intersection away from the nucleus and ending when the trajectory reaches the detector. There is a slight difference from the classification defined by Mitchell and Delos. In their classification, they end the record when the trajectory encircles the nucleus for the last time. Counting the total number of intersections with the negative axis after the encircling of the nucleus for the last time is important, as trajectories at different intersections with the axis after the encircling of the nucleus for the last time make different contributions to the interference pattern. Figure 1 shows some typical trajectories in our calculation. For example, for the orbit starting at angle $\theta = 0.71$, the label $o(-)^2$ means that the orbit encircles the nucleus once before it intersects the negative z axis for the first time, and then it intersects the negative z axis twice more without encircling the nucleus. In the notation by Mitchell and Delos, this orbit would be labeled as o.

III. RESULT AND DISCUSSION

We calculate the spatial distribution of electrons arising in photoionization microscopy of a hydrogen atom in parallel electric and magnetic fields, at $B = 4$, $E = 0$, which is shown in Fig. 2. It can be seen that the radial distribution has

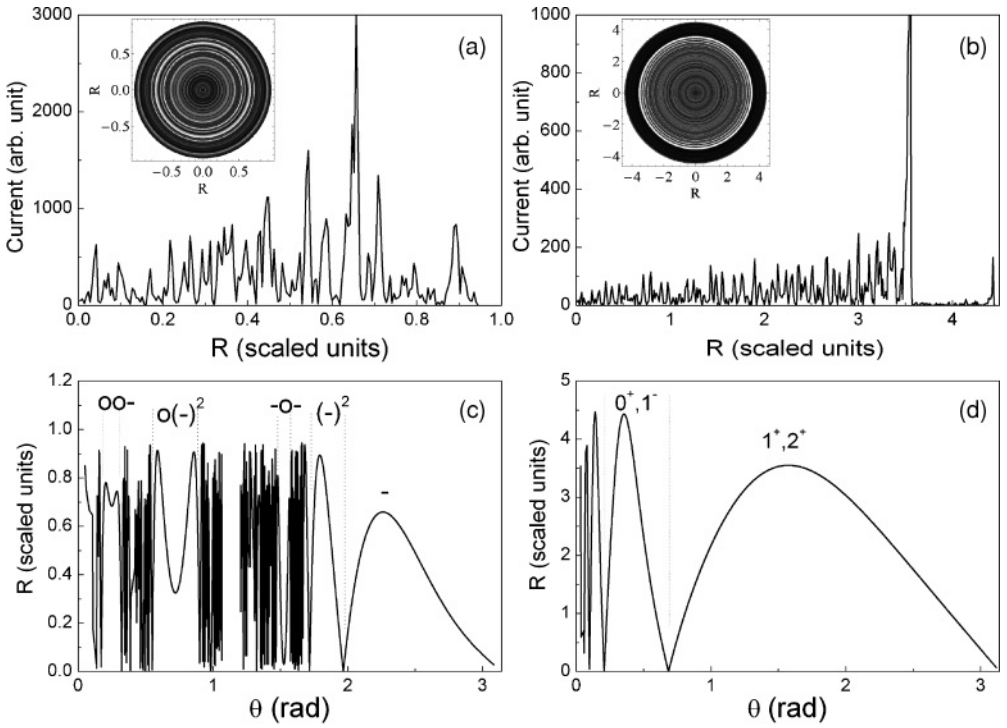

FIG. 2. The calculated photoionization microscopies of a hydrogen atom in parallel electric and magnetic fields and in a pure electric field. Upper panels: the radial distribution of the flux of electrons striking the detector located at $z = -4$ on the detector at scaled energy $E = 0$ of a hydrogen atom in parallel electric and magnetic fields in a scaled magnetic field of $B = 4$ (a) and in a static electric field (b). Lower panels: the dependence of the radius of impact on the detector on the initial angle θ at which the trajectory is launched. (c) and (d) correspond to (a) and (b), respectively. The dashed lines connect each of escape segments to their corresponding patterns.

two-pattern structures, for example, for R close to but slightly less than 0.6605, two trajectories having $(-)$ structure contribute the inner oscillations, and for R slightly less than 0.8973, two trajectories with $(-)^2$ structure give the dominant contribution to the outer oscillations as depicted in Fig. 2(a). This feature is similar to the case of a pure electric field, which is displayed in Fig. 2(b) for comparison.

In the latter case, the inner intense pattern arises predominantly from the interference between the trajectories 0^+ and 1^-, corresponding to direct ionization, and the outer pattern to the indirect trajectories corresponding to indirect ionization, mainly 1^+ and 2^+, following the notation of Kondratovich and Ostrovsky [4,30]. The two-pattern structure implies two primary groups of trajectories, and these arise from the Coulomb interaction of the electron with the ion. This interaction causes the electron trajectories to experience a significant deflection from the parabolic tracks they would follow in an electric field if the Coulomb field were not present [6].

When the parallel magnetic field is added to the constant electric field and the Coulomb field, the maximum radius of each pattern is slightly smaller than that of the hydrogen atom in a pure electric field, as the magnetic field restricts the motion of the electron in the plane perpendicular to the z axis [28,31]. The number of fine scale maxima of the inner pattern decreases because the semiclassical phase differences between two $(-)$ trajectories decrease when the magnetic field is employed. The magnetic field causes electrons to oscillate perpendicular to the field more rapidly compared to the case of a pure electric field. The trajectories are not at all comparable to parabolas, and the direct trajectories corresponding to the case of a pure electric field are strongly affected by the magnetic field. Some of them play their roles as in the case of a pure electric field but they have to cross the negative z axis once. Some of them pass the negative z axis twice. They have the structure $(-)^2$ and correspond to the main indirect trajectories in the case of a pure electric field (for example, 1^+ and 2^+) [4,30]. Some trajectories with smaller ejected angles encircle the core at least once before they land on the detector, such as $-o-$, but unlike the case of pure electric field, they play very important roles, which will be discussed later. All of these trajectories correspond to different patterns and the interference of these patterns makes the microscopy of a hydrogen atom in parallel electric and magnetic fields very complex, as shown in Fig. 2(a). We can also see that in Fig. 2(c), in our case, the function of radius $R(\theta)$ on the detector becomes more complicated and exhibits fractal structure as well as a certain self-similarity, which is similar to the epistrophic self-similarity introduced by Mitchell and Delos when treating the escape-time dynamics in the ionization [26,27]. Additionally, after the magnetic field is introduced, more critical angles θ_i will generate orbits which contribute to the impact electron current at $R = 0$. Thus, the recorded electron counts at $R = 0$ increase dramatically [1].

Some typical interference patterns with prominent contributions for the final radial distribution on the detector in our case are shown in Fig. 3. They are obtained by calculating the amplitude by restricting the domain of ejection angles to an appropriate region as shown in Fig. 2(c). Like the direct and indirect trajectories in a pure electric field, trajectories $(-)$ and trajectories $(-)^2$ lead to two completely different structures, with much smaller fringe spacing in the $(-)^2$ component. The $(-)$ electron signal dominates the signal in the inner region of the image, while the trajectories $(-)^2$ give only a weak signal but their high spatial frequency makes a strong modulation for

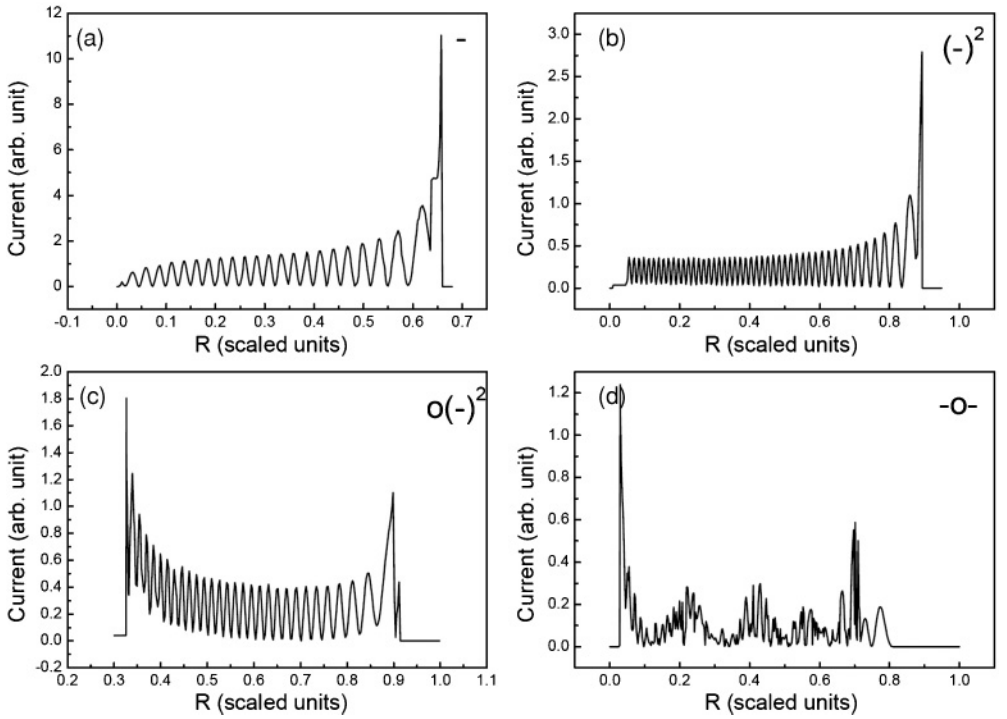

FIG. 3. The radial distributions of the flux of electrons striking the detector located at $z = -4$ on the detector at scaled energy $E = 0$, $B = 4$ for a hydrogen atom in parallel electric and magnetic fields, corresponding to trajectories with different structures: (a) $(-)$, (b) $(-)^2$, (c) $o(-)^2$, and (d) $-o-$ as shown in Fig. 2(c).

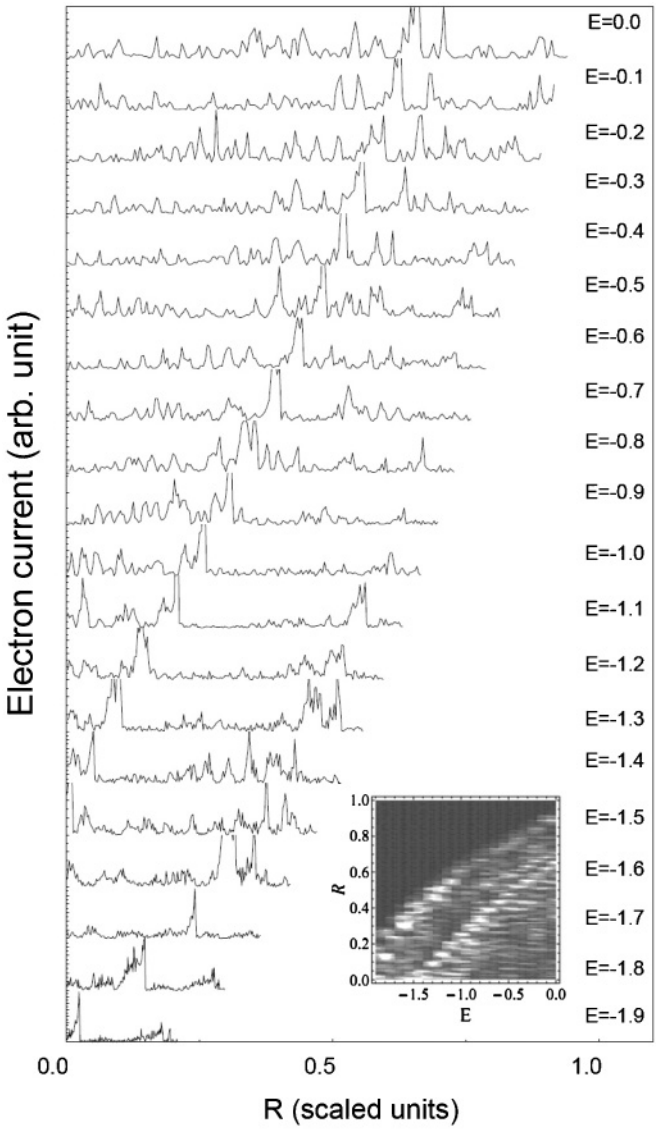

FIG. 4. Radial distribution of the electron current at various energies from saddle-point energy $E_{sp} = -2$ to energy $E = 0$ in parallel electric and magnetic fields with $\widehat{F} = 19$ V cm^{-1}. The density of the electron current is plotted in coordinates (E,R) as shown in the inset.

the radial distribution. They are displayed in Figs. 3(a) and 3(b). The pattern in Fig. 3(c) results from the interference of four trajectories with $o(-)^2$ structure. Unlike the above two patterns in Figs. 3(a) and 3(b), this pattern has a well-liked structure with a minimum in the center of the pattern and it has a fringe spacing similar to the pattern corresponding to the trajectories $(-)^2$. This kind of pattern makes no contribution to the inner region, but strongly modulates the whole region $0.332 < R < 0.9067$. This family of orbits originates from the ejected angles whose values are between those for the direct and indirect orbits in the case of an atom in a pure electric field. In Fig. 3(d) is the pattern corresponding to the interference of trajectories with the structure $-o-$. This pattern is more complicated. It has a four-term interference structure in the region $0.0346 < R < 0.7140$, and a two-term interference structure in the region $0.7140 < R < 0.8089$. The four-term interference structure shows large oscillations with low spatial frequency together with weaker but fast oscillations.

The radial distribution of the electron current depends on the excitation energy because the contributing trajectories change with energy [4,14]. In Fig. 4 is shown a series of radial distributions of the electron current at $B = 4$ within a range of excitation energies varying from $E = E_{sp} = -2$ to $E = 0$. The patterns corresponding to the trajectories $(-)$ and $(-)^2$ have similar smooth evolutions with the scaled energy, as expected for the assumption of an isotropic initial distribution of the ejected angles. The contribution of the trajectories $(-)$ begins to take effect at $E_c \approx 0.77E_{sp}$, which is similar to the direct trajectories in the case of a pure electric field [4]. This kind of trajectory always begins with large ejection angles (i.e., in the down-field direction) and has a crossing with the z axis only once. The motion of electrons with a smaller ejection angle is extremely complex; there is fractal structure within structure at all levels of resolution, and new families of trajectories appear as the energy changes. Figure 4 gives some idea of the complexity of the system.

IV. CONCLUSION

We have performed a theoretical calculation of the spatial distribution of electrons arising from photoionization microscopy of hydrogen atoms in external parallel electric and magnetic fields, and we have analyzed the interference patterns corresponding to trajectories with different structures. The calculation is based on the approximation that electrons are ejected isotropically in all directions, implying that only the so-called background contribution introduced by Kondratovich and Ostrovsky is considered. Besides the two main interference patterns observed in the the case of a pure electric field, new patterns emerge in the case of the hydrogen atom in parallel electric and magnetic fields. These patterns are connected with the very complex structure of trajectories that appear when parallel fields are combined with a Coulomb field.

ACKNOWLEDGMENTS

The authors acknowledge Professor J.-P. Connerade in Imperial College, London, for the beneficial discussion. This work is supported by National Natural Science Foundation of China (NSFC) under Grant No. 10774162, and by the U.S. National Science Foundation. We thank L. B. Zhao for some helpful calculations.

[1] C. Blondel, C. Delsart, and F. Dulieu, Phys. Rev. Lett. **77**, 3755 (1996).
[2] C. Blondel, C. Delsart, F. Dulieu, and C. Valli, Eur. Phys. J. D **5**, 207 (1999).
[3] C. Bordas, Phys. Rev. A **58**, 400 (1998).
[4] F. Lépine, C. Bordas, C. Nicole, and M. J. J. Vrakking, Phys. Rev. A **70**, 033417 (2004).
[5] C. Nicole, H. L. Offerhaus, M. J. J. Vrakking, F. Lépine, and C. Bordas, Phys. Rev. Lett. **88**, 133001 (2002).

[6] C. Nicole, I. Sluimer, F. Rosca-Pruna, M. Warntjes, M. Vrakking, C. Bordas, F. Texier, and F. Robicheaux, Phys. Rev. Lett. **85**, 4024 (2000).
[7] Y. N. Demkov, V. D. Kondratovich, and V. N. Ostrovsky, JETP Lett. **34**, 403 (1981).
[8] V. D. Kondratovich and V. N. Ostrovsky, J. Phys. B **17**, 1981 (1984).
[9] V. D. Kondratovich and V. N. Ostrovsky, J. Phys. B **17**, 2011 (1984).
[10] V. D. Kondratovich and V. N. Ostrovsky, J. Phys. B **23**, 3785 (1990).
[11] T. Kramer, C. Bracher, and M. Kleber, Europhys. Lett. **56**, 471 (2001).
[12] C. Bracher, T. Kramer, and J. B. Delos, Phys. Rev. A **73**, 062114 (2006).
[13] C. Bracher and J. B. Delos, Phys. Rev. Lett. **96**, 100404 (2006).
[14] C. Bordas, F. Lépine, C. Nicole, and M. J. J. Vrakking, Phys. Rev. A **68**, 012709 (2003).
[15] F. Texier, Phys. Rev. A **71**, 013403 (2005).
[16] L. B. Zhao and J. B. Delos, Phys. Rev. A **81**, 053417 (2010).
[17] L. B. Zhao and J. B. Delos, Phys. Rev. A **81**, 053418 (2010).
[18] P. A. Braun and E. A. Solov'ev, Sov. Phys. JETP **59**, 38 (1984).
[19] P. Cacciani, E. Luc-Koenig, J. Pinard, C. Thomas, and S. Liberman, J. Phys. B **19**, L519 (1986).
[20] P. Cacciani, E. Luc-Koenig, J. Pinard, C. Thomas, and S. Liberman, Phys. Rev. Lett. **56**, 1467 (1986).
[21] K. Richter, D. Wintgen, and J. S. Briggs, J. Phys. B **20**, L627 (1987).
[22] J.-M. Mao, K. A. Rapelje, S. J. Blodgett-Ford, J. B. Delos, A. König, and H. Rinneberg, Phys. Rev. A **48**, 2117 (1993).
[23] M. Courtney, Phys. Rev. A **51**, 4558 (1995).
[24] K. A. Mitchell, J. P. Handley, B. Tighe, J. B. Delos, and S. K. Knudson, Chaos **13**, 880 (2003).
[25] K. A. Mitchell, J. P. Handley, B. Tighe, J. B. Delos, and S. K. Knudson, Chaos **13**, 892 (2003).
[26] K. A. Mitchell, J. P. Handley, B. Tighe, A. Flower, and J. B. Delos, Phys. Rev. A **70**, 043407 (2004).
[27] K. A. Mitchell, J. P. Handley, B. Tighe, A. Flower, and J. B. Delos, Phys. Rev. Lett. **92**, 073001 (2004).
[28] C. Bracher and J. B. Delos, Phys. Rev. Lett. **96**, 100404 (2006).
[29] K. A. Mitchell and J. B. Delos, Physica D **229**, 9 (2007).
[30] V. D. Kondratovich and V. N. Ostrovsky, J. Phys. B **23**, 21 (1990).
[31] S. Gao, G. C. Yang, S. L. Lin, and M. L. Du, Eur. Phys. J. D **42**, 189 (2007).